ECN

Energy research Centre of the Netherlands

Performance Analysis of a Shrouded Rotor for a Wind Powered Vehicle

K. Boorsma

L.A.H. Machielse

H. Snel

Paper presented at

Torque 2010, June 28-30, Heraklion, Crete, Greece

ECN-M-10-088 NOVEMBER 2010

Performance Analysis of a Shrouded Rotor for a Wind Powered Vehicle

Koen Boorsma
Energy research Center of the Netherlands, ECN
P.O. Box 1, 1755 ZG Petten
boorsma@ecn.nl

Leo Machielse
Energy research Center of the Netherlands, ECN
P.O. Box 1, 1755 ZG Petten
machielse@ecn.nl

Herman Snel
Energy research Center of the Netherlands, ECN
P.O. Box 1, 1755 ZG Petten
snel@ecn.nl

Abstract

This paper presents some design aspects of a wind powered vehicle. Special attention is paid to the specification of the diffuser-rotor combination. The performance of this combination is verified by means of wind tunnel testing. The optimal pitch angle is determined and the influence of roughness and rotor misalignment is investigated. In addition to that, several additions to enhance rotor performance have been researched. The successful test campaign has resulted in a valuable database for use in wind powered vehicle design and beyond.

Keywords: Wind powered vehicles, rotor aerodynamics, diffuser, wind tunnel

1 Introduction

In August 2008, ECN participated in a race for wind propelled cars in Den Helder, the Netherlands. Cars of various designs competed for the highest speed in a race against the wind.
The ECN car - called *Impulse* – was propelled by an “engine” consisting of a purposefully designed 3-bladed rotor within a diffuser.
The *Impulse* has been very successful in the race. In head wind with an average velocity of 9.3 m/s a vehicle speed of 53% of the wind velocity was reached, good enough for the second prize in the speed competition.
Later on, the same configuration of diffuser and rotor has been tested in the Open Jet Facility (OJF) of Delft University of Technology.

Firstly some design requirements are addressed. Special attention is paid to the design of the diffuser-rotor combination, including predicted performance. Then the wind tunnel measurements are described and the results are compared with the design predictions. Finally the measured data is used to predict the car performance, which is compared to the actual performance during the race. On this basis an estimate is given of the performance potential using the current rotor diffuser combination.

Figure 1: The *Impulse* driving on the race track, a sea dike in Den Helder, the Netherlands.

2 Wind powered vehicle

The rotor of a wind powered vehicle produces power but also adds to the total drag. On a horizontal track and at constant car velocity U in head wind V the useful power P_u is at equilibrium with the power losses due to the trust T, the aerodynamic drag of the car body D and the rolling resistance R in the wheels and the friction with the ground.

$$P_u = U (T + D + R) \quad (1)$$

where:

$$P_u = \eta C_P 0.5 \rho (V + U)^3 A \quad (2)$$

$$T = C_T 0.5 \rho (V + U)^2 A \quad (3)$$

$$D = 0.5\ \rho\ (V + U)^2\ (A_D + A_o) \quad (4)$$

$$R = f\ M\ g \quad (5)$$

with:

A	rotor area
A_D	drag area of the car body
A_o	drag area of other components (mesh, mast, ..)
C_P	power coefficient
C_T	thrust coefficient
f	friction coefficient (wheels and ground contact)
g	gravitational constant
M	mass of car and driver
U	car speed
V	wind speed
η	drive train efficiency
ρ	air density

Assume that the aerodynamic drag of the car body and the rolling resistance are negligible compared to the rotor thrust. In that case the equilibrium condition results in:

$$U/V = (C_P/C_T) / (1/ \eta - C_P/C_T) \quad (6)$$

With this assumption high vehicle speeds are reached at high drive train efficiency η and high C_p/C_T values. So an important goal in the design is to achieve high values for these parameters within the restrictions that were imposed by the organizer of the race like restrictions for the width and height of the car to 2 m and 3.5 m respectively and the rotor area to 4 m^2. Further the safety requirements demanded containment of the rotor in a safety cage or net with a maximum mesh of 0.1 m.

A more elaborate investigation into the performance of wind driven vehicles including a simple one point optimization method, based on the Blade Element Momentum theory, can be found in [1].

3 Rotor and diffuser

3.1 Design

Despite the advantages of a VAWT (absence of a yaw mechanism and the possibility to realize the largest single rotor area with straight blades), the HAWT concept was chosen. The main reasons were the superior performance coefficient that should compensate for the difference in rotor area and the possibility to use a diffuser for performance enhancement and as supporting ring for the required safety cage as well. Furthermore it was decided to use a 3-bladed rotor for smooth running, less vibrations and low rotational speed.

As mentioned above, safety requirements for the race led tot the use of a shroud around the rotor. This shroud was given the shape of a diffuser, to augment the mass flow through the rotor. The diffuser geometry was chosen based on the following considerations.

- A long diffuser would lead to a small rotor, due to the maximum diameter of the combination;
- A NACA 44 series aerfoil was chosen because of the decent behavior at low Reynolds numbers;
- A small opening angle of the diffuser was chosen, because of the low Reynolds number and the danger of separation;

The final choice was made for a diffuser chord length of 25 cm and an opening angle of 5 degrees. The chord based Reynolds number at 10 m/s speed is then 1.7×10^5.
The flow augmentation due to the diffuser was calculated with a lifting surface program for the circular geometry and the NACA 44 series camber line, using 10 vortex elements on the chord. Figure 2

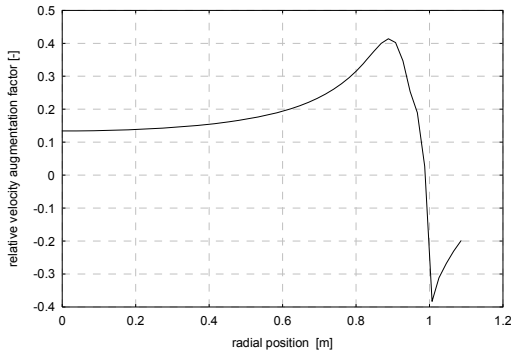

Figure 2: The calculated flow field at 10 cm behind the opening of the diffuser.

shows the result of the calculations. The area reduction due to the diffuser is approximately 4%, but the calculated augmented volume flow equals 22%, so that the net effect should be positive. For the adapted design of the rotor, the augmented velocities were multiplied by a conservative, but rather arbitrary factor of 0.7, to account for decambering effects resulting from the low Reynolds number.

Generally, such arbitrary approximation was driven by the need of results in the minimum time possible.

Preliminary analysis revealed an optimal induction coefficient of 0.15 for the assumed drive train efficiency and other losses. The rotor geometry was designed for this coefficient at a tip speed ratio of 5 and including the flow augmentation factor, in order to have a large C_P/C_T ratio, needed for the specific purpose. As a design effective incoming speed, a value of 11 m/s was used, composed of free wind speed, the speed of the car and the shroud augmentation. This would give a rotor blade chord Reynolds number of almost 3 x 10^5. A NACA 4415 profile was chosen for the entire rotor, and the aerodynamic data for the Reynolds number were obtained from RFOIL [5].
The resulting geometry was adapted for the manufacturing process into the result shown in Figure 3. The blades were shortened to 950 mm, to ensure sufficient distance from the shroud surface.

radius [mm]	chord [mm]	twist [°]
975	45	4.5
878	52.5	5.7
780	57	7.1
683	62	8.8
585	69	10.8
488	78.9	13.7
390	95	17.7
293	112	23.4
195	132	32.5
98	140	46.5

Table 1: Chord and twist distribution of the rotor blades. The blade tips have been cut off at a length of 950 mm.

3.2 Manufacture

The blades were cut from a solid 6061 T6 Aluminum cylinder in a CNC milling machine according to the calculated geometry. There was no time for optimization of the milling process which is difficult for such a slender product. As a result the thickness and chord distribution of the blades deviated from each other. The resulting chord and thickness distributions are shown in Figure 3 and 4.
The rotor mass distribution has been balanced but the blade geometry has not been corrected. For simplicity the blades were fixed during the race though the blade pitch angle could be adjusted in advance depending on the expected wind conditions.
The diffuser is CNC milled out of a ring of laminated plates of AxonProlab 65 mould material.

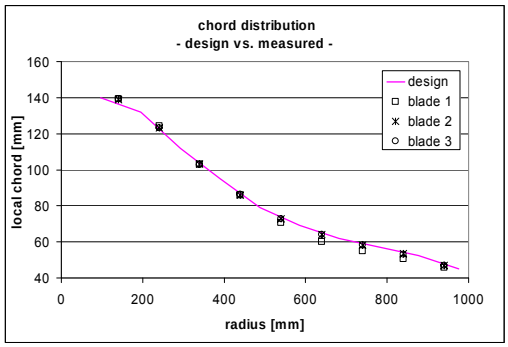

Figure 3: Measured chord distribution of the blades compared to the design values

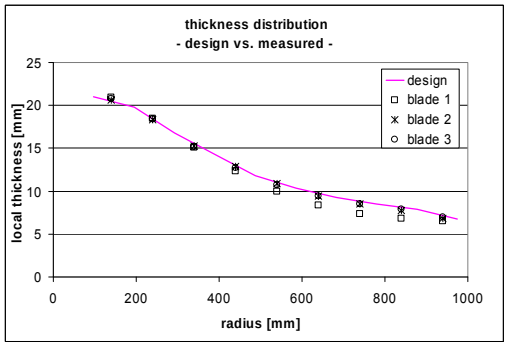

Figure 4: Measured thickness distribution of the blades compared to the design values

4 Experimental arrangement

4.1 Model

For the wind tunnel test the assembly consisting of rotor-diffuser, upper gear box and yaw tube, have been mounted on a cylindrical mast of equal diameter (130 mm) to the *Impulse*.
The tower is supported by four legs on a ground plate and provided with a yawing mechanism for directing the rotor at different angles with the tunnel flow.

Within the rotor area the yaw tube is provided with a tail featuring a 36 cm long triangular cross-section extension for streamlining purposes. The diffuser is supported by 2 streamlined Aluminum struts of 31.75 mm thickness and 79.5 mm chord at 60 degrees with the vertical and a vertical steel pole of 10 mm diameter. At the front and the back the diffuser is provided with of a mesh of 2 mm diameter

steel wire. The spacing between the wires is about 0.1 m.
The length of the wire at one side of the diffuser is 29 m. In front of the rotor cable terminals are used for fastening the wire to the nose of the diffuser. The connections between wire and diffuser are flush at the back side.
The straight axis of the upper angular gear directly drives a permanent magnet DC generator. The generator is mounted on a support. The electric load for the DC generator was realized in an array of resistors. By using parts of the resistors and applying series and parallel connections different values for the resistance could be obtained in order to vary the rotational speed of the rotor.

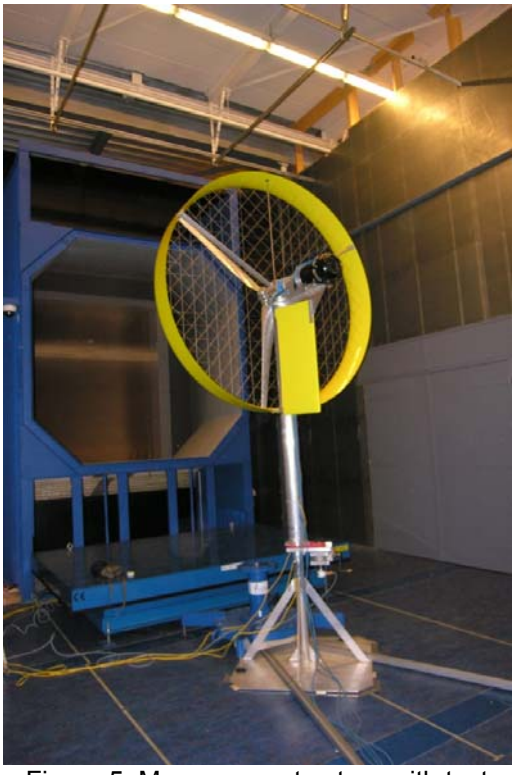

Figure 5: Measurement set-up with test model positioned in front of the wind tunnel nozzle.

4.2 Test set-up

The model was positioned in the test section of the newly built Open Jet Facility (OJF) of Delft University of Technology. The OJF is a closed loop tunnel with a test section (h x w x l = 6.0 m x 6.5 m x 13.5 m) featuring an open jet configuration. An octagonal nozzle with an equivalent diameter of 3 m produces a jet that is collected at the porous rear test section wall. The setup is illustrated in Figure 5. The vertical position of the rotor center was aligned with the nozzle center (3 m above the test section floor) and the axial distance between rotor plane and nozzle exit amounted to 3 m. This ensured minimum nozzle blockage whilst preventing interference of the jet shear layer with the model. At the time of writing the flow quality of the tunnel (i.e. uniformity and turbulence intensity) had not been measured yet, although the application of anti-turbulence screens makes for an expectation of intensities below 0.5%.

4.3 Apparatus

4.3.1 Tunnel variables

The tunnel speed has been determined by using the pressure difference over two pressure sensors located in the nozzle contraction. A calibration has been performed with a pitot tube at the model center location (for an empty tunnel) to determine the relationship between tunnel speed and pressure difference.
To quantify the dynamic head of the flow, the air density is determined using the barometric pressure and temperature of the tunnel.

4.3.2 RPM and torque

Between gear box and generator a torque transducer and a pulse generator were installed for measuring rotor torque and rotational speed. Because of this set-up the net rotor torque can be obtained by correcting for the bearing losses in the gear box.

4.3.3 Axial force

The tower of the test model is provided with a strain gauge bridge for measuring the bending moment. Only the moment in flow direction was measured. The bridge has not been calibrated but the bending moment is calculated directly from the tower dimensions (diameter 130 mm, wall thickness 5 mm) and the bridge and strain gauges properties.

4.3.4 Tufts (‘Tell tales’)

Small dark blue colored woolen threads of approximately 6 cm length were mounted around the circumference of the inner surface of the shroud, the wired mesh and the tower extension. This allowed for monitoring separated flow features, especially in the case of yawed flow.

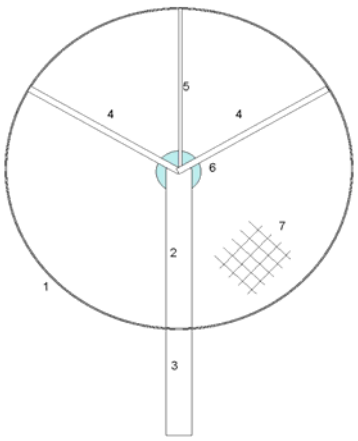

n	component	C_d, C_{do}	Refe-rence	length	Dimen-sion	Area	Drag area
		[-]		[m]	[m]	[m^2]	[m^2]
1	diffuser	0.015	XFOIL	6.180	0.250	1.545	0.023
2	cylinder with tail	0.890	[2]	0.960	0.130	0.125	0.111
3	cylinder	1.200	[2]	0.450	0.130	0.059	0.070
4	streamlined strut	0.500	[2]	0.890	0.032	0.057	0.028
5	cylinder	1.200	[2]	0.880	0.010	0.009	0.011
6	nacelle	0.820	[2]		0.210	0.035	0.028
7	wire mesh	1.140	[2]			2.835	0.140
					Total drag coefficient (ref rotor area)		**0.145**

Figure 6: Breakdown of axial force contribution

The signals for torque, rotor speed and bending moment were sampled with DANTE data acquisition system of ECN, converted into physical units, recorded and displayed.

4.4 Data reduction

4.4.1 Breakdown of axial force

In order to determine the axial force on the rotor, the contributions of shroud, tower and the several struts have to be removed. Figure 6 gives an estimate of the drag breakdown of these components, using the book of Hoerner [2].

In addition to the estimate, axial force measurements have been performed at rotor standstill. The blades were turned to vane position and the rotor azimuth angle was fixed at 60 degrees. Hence the blades were positioned in front of the tower and the struts holding the diffuser respectively.

The measured drag is considerably higher than the estimated contribution. Most probably this is mainly due to interference effects. The velocity dependency visible in Figure 7 can be attributed to the cylinder that crosses the critical Reynolds number region. Since the measured data is believed to represent the contribution of shroud, struts and cylinder better than the estimation, this data is used for correcting the axial force.

4.4.2 Wind tunnel boundary effects

Since the rotor area is significant compared to the jet area, a correction for wind tunnel boundary effects is applied. The correction can be divided into nozzle blockage and solid blockage effects as described in [3].

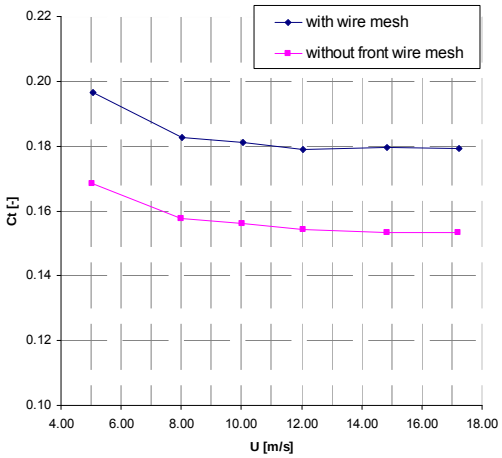

Figure 7: Axial force at rotor standstill

The proximity of the model to the nozzle results in nozzle blockage and changes the dynamic-pressure measuring system from the empty-tunnel value. By approximating the model as a bluff body with frontal area equal to the rotor area, an estimate of approximately 1% tunnel speed increase is obtained.

For the solid blockage, the method of Glauert for a propeller in a closed wall wind tunnel as described in [4] is adopted. According to the authors of [4], the solid blockage of a bluff body in an open jet roughly amounts to a quarter of the solid blockage in a closed tunnel. However the sign of the blockage should be inverted, since the model induced jet expansion lowers the tunnel speed at the model location. The axial force coefficient C_T that was used in this correction does not include the contribution of the shroud, tower and struts. The solid blockage due to these components is neglected.

Since the collector inlet approximately has the dimension of the rear test section wall, collector blockage effects are not expected to be of importance here. In addition to that, empty tunnel pressure gradients are not considered.
Combining the above described corrections yields a change of tunnel speed between -1.5% and 1.3%, dependent on the axial force.

4.4.3 Processing of corrected quantities

The corrected torque and axial force are reduced to non dimensional C_P, C_T and C_P/C_T values using the corrected freestream velocity U, rotor area and air density. The rotor area used for this reduction does not include the shroud and hence is based on a rotor diameter of 1.9 m instead of 2.0 m. The ideal gas law is used to process the measured pressure and temperature values to air density.
The values are presented as a function of tip speed ratio lambda, which is the ratio of rotational speed at the tip and the freestream velocity.

4.5 Test matrix

A variety of configurations was tested. The main aim was to determine the rotor characteristics. An important subject of parameter variation is the pitch angle of the blades. In addition to that the effect of roughness and yaw on rotor performance is assessed. The effect of the wire mesh and the tower streamline has also been subject of investigation. Unfortunately the time schedule did not allow for removal of the shroud in order to determine its effect on rotor performance. All of the tests have been performed for a variety of tunnel speeds ranging from 5 to 15 m/s. Using an average driving velocity of half the wind speed for the Impulse, this corresponds to winds between 3 and 5 Beaufort. The RPM of the rotor for these wind speeds varied between 250 and 850 to obtain tip speed ratios between 3 and 8.
To determine the rotor characteristics, the rotational speed was varied using the resistors described in section 4.1, for a constant wind tunnel speed and pitch angle. Prior to the measurement of each data set, the rotor was kept spinning at constant wind speed until the measured torque stayed constant. This ensured the bearing losses not to vary due to heating up throughout the measurements.

The reproducibility of each obtained data set was checked by finishing with a repetition of the first rotational speed.

5 Results

5.1 Reynolds number effects

Comparing the non-dimensional curves for various freestream velocities yields the trends given in Figures 9 to 11.
The effect of Reynolds number on the profile aerodynamics is investigated using RFOIL [5] as illustrated in Figure 8 for the range under consideration.

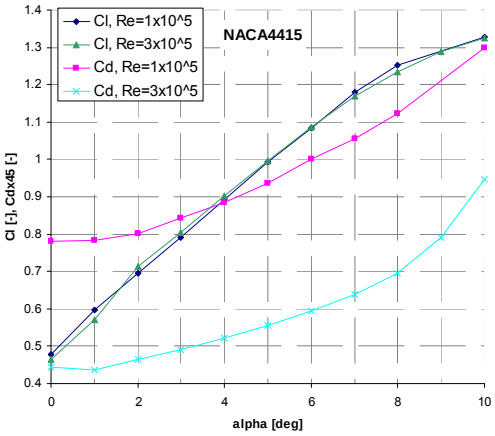

Figure 8: Influence of Reynolds number on NACA4415 profile characteristics

The increase in frictional drag by forward creeping transition is overshadowed by the pressure drag decrease due to the thinning boundary layer. However the lift is hardly affected by the decreasing boundary layer displacement. Hence the C_T-lambda curves coincide for different freestream velocities, whilst the C_P-lambda curves are shifted upward for increasing tunnel speed.

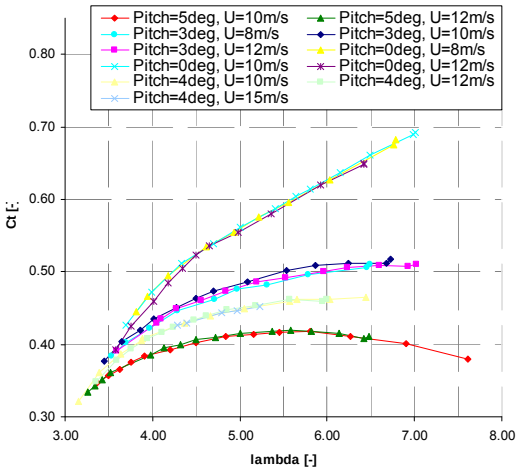

Figure 9: Measured C_T values

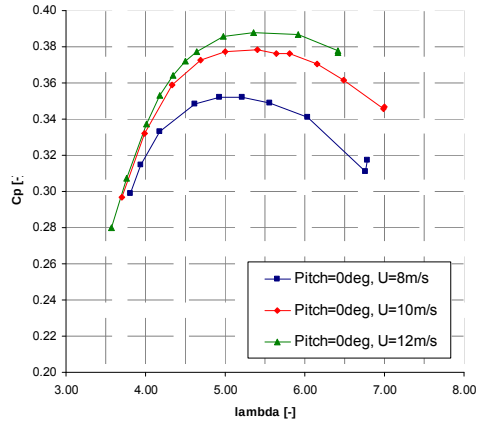

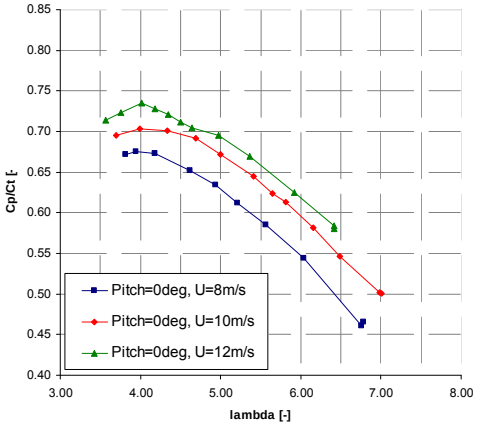

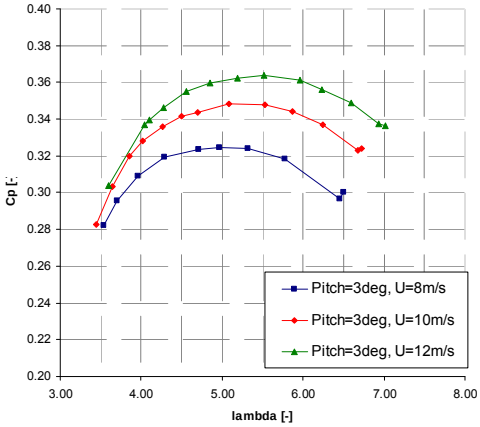

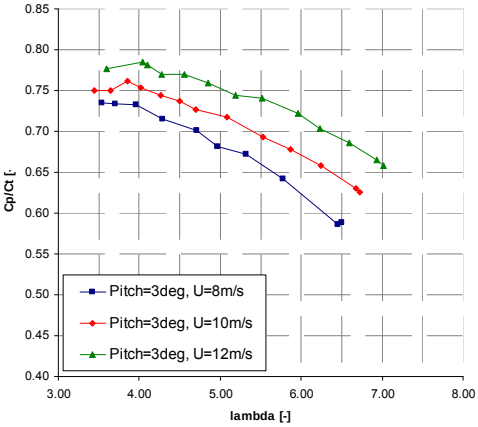

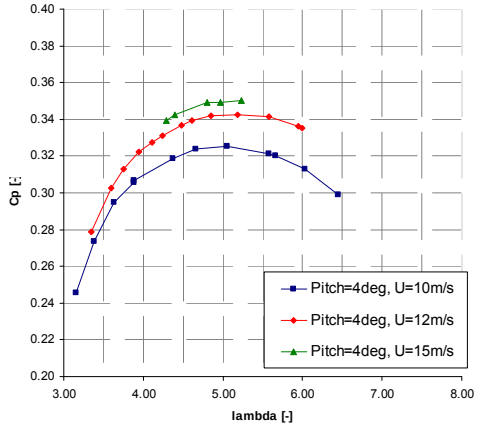

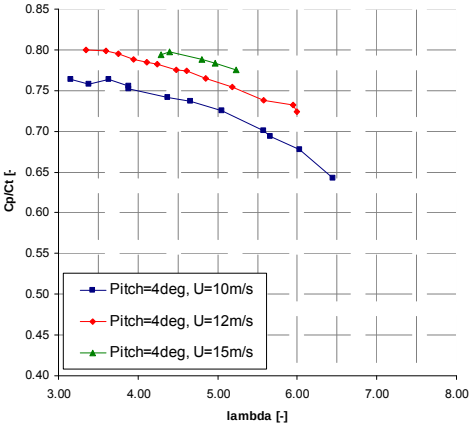

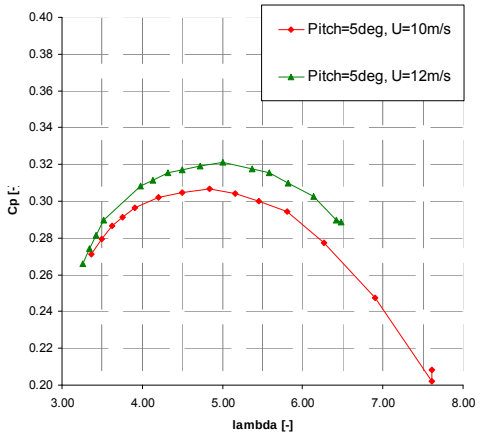

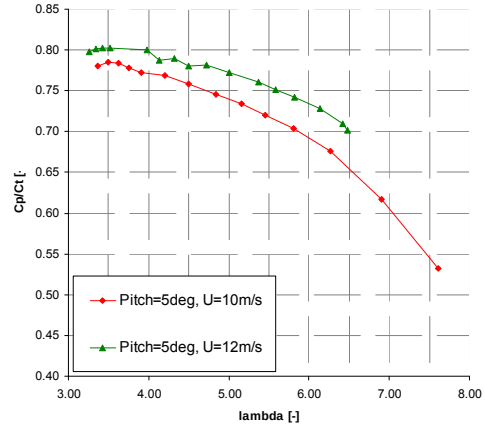

Figure 10: Measured C_P values

Figure 11: Measured C_P/C_T values

5.2 Pitch angle

The influence of pitch angle is depicted in Figures 12 and 13. The trend for U=10 m/s is similar to the trend in the remainder of the tunnel speeds. The Figures clearly illustrate that although the power is significantly higher for a pitch angle of 0 degrees, the accompanied increase in rotor thrust diminishes the C_P/C_T ratio. A pitch angle of 5 degrees seems to yield the best ratio, although the difference is small with 3 and 4 degrees. The maximum ratio is achieved at a relatively low tip speed ratio (~4) compared to the lambda at maximum C_P (~5.5).

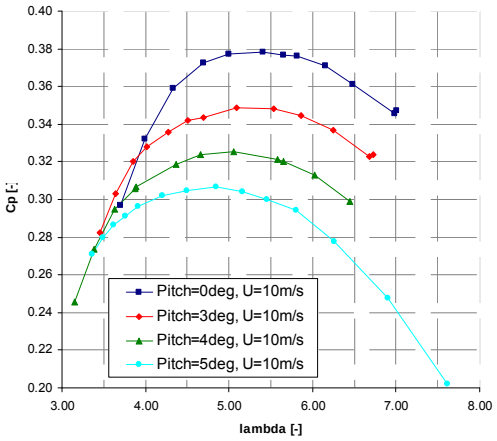

Figure 12: Influence of pitch angle on C_P

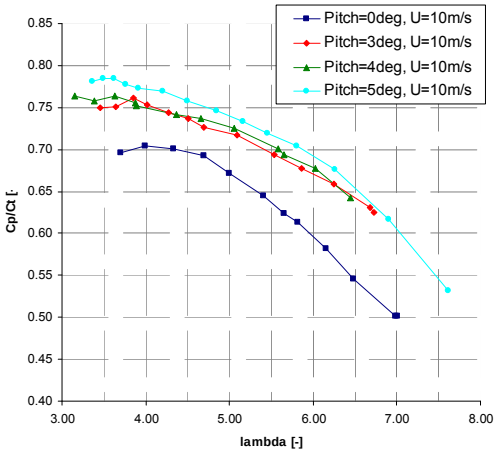

Figure 13: Influence of pitch angle on C_P/C_T

5.3 Roughness

The influence of roughness on the blades was assessed by application of two different types of roughness strips. The first type with a width of 16 mm and a thickness of 0.8 mm was cut out of P60 sandpaper. The second type was cut out of 0.29 mm thick smooth surfaced tape featuring 45 degree angle serrations on the side facing the flow. The width of the serrations was 5 mm. The strips were applied along the span of the blades at a chord wise distance of 15% chord on both pressure and suction side. The results are shown in Figure 14 to 16 for a pitch angle of 4 degrees.

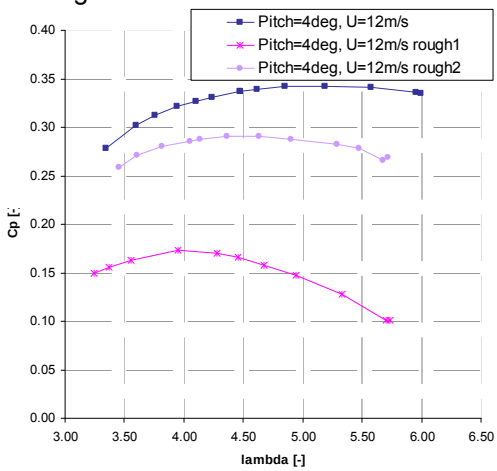

Figure 14: Influence of roughness on C_P

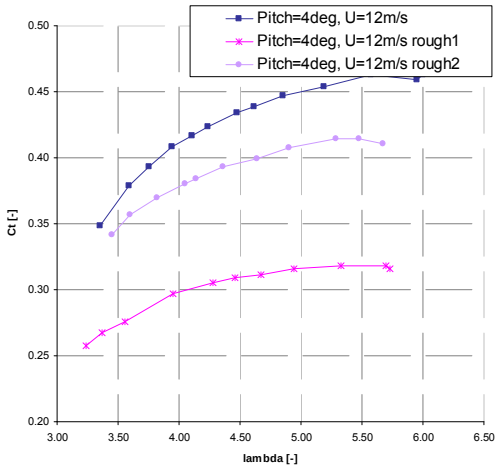

Figure 15: Influence of roughness on C_T

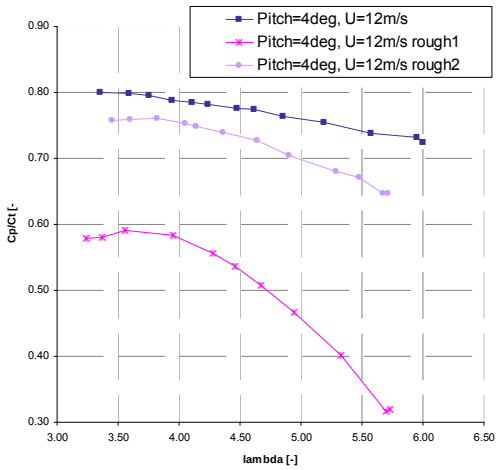

Figure 16:Influence of roughness on C_P/C_T

The effect of the first strip is rather large, owing to its large thickness. The effective airfoil shape and thus profile characteristics are altered significantly. Increase in profile drag and decrease in lift is causing a decrease in C_P and C_T respectively. The optimum Cp location shifts from a tip speed ratio of 5.5 to 4. The maximum value of C_P/C_T is decreased by 20%.
The effect of the second strip is less strong but the observed trends are in qualitative agreement with the first strip. The strip is comparable to more conventional tripping devices, merely causing the boundary layer to be turbulent without inducing an excessive boundary layer momentum loss.

5.4 Rotor misalignment

The effect of rotor misalignment was assessed by turning the rotor stepwise into the wind for a constant resistance at lambda≈4. The results are illustrated in Figure 17. A misalignment of 5 degrees does not significantly affect rotor performance. Although the power coefficient stays approximately constant up to a yaw angle of 12 degrees, the axial force increases above 5 degrees and thereby reduces the C_P/C_T ratio. Increasing the misalignment above 20 degrees kills the rotor speed and thus the power, while only a 'standstill' axial force contribution remains comparable to Figure 7.

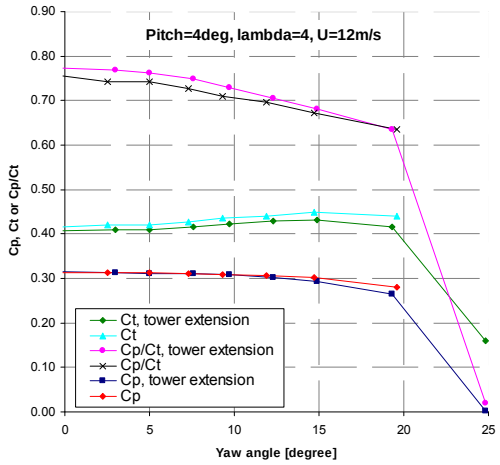

Figure 17: Influence of rotor misalignment

Streamlining the tower by means of the tail described in section 4.1 negatively affects the power in yaw. Since the tail is not aligned with the undisturbed flow direction in yaw, the power decreases although the difference in axial force (in rotor axial direction) is hardly affected. Tufts on the towertail suction surface indicated flow separation from 5 degree yaw angle onwards.

5.5 Performance enhancement

5.5.1 Shroud

As outlined in section 3.1, the opening angle of the shroud was chosen rather conservatively at 5 degrees because of the danger of separation. Flow separation for various yaw angles was monitored by tufts on the inside surface of the upwind side of the shroud. These tests have been performed at U=10 m/s and a pitch angle of 5 degrees, for both rotor stand still as well as a spinning rotor (around 400 rpm). The tufts at rotor center height are obviously most representative for mimicking an increase of the shroud opening angle.
It appeared that flow separation based on these tufts exists only from 19 degrees and 23 degrees yaw onwards for rotor standstill and the spinning rotor respectively. However, the tufts located above or below rotor center height feature flow separation from 7 and 16 degrees yaw onwards for rotor standstill and the spinning rotor respectively. Most probably the spinning rotor energizes the boundary layer, resulting in higher separation angles.
Although extrapolation of these test results to a new opening angle is not straightforward, they indicate that increasing this angle certainly is an option. Although the shroud is expected to increase the mass flow through the rotor and hence augment the power, the same holds for the axial force. According to Jamieson [6], the effect of the shroud would cancel out for the C_P/C_T ratio, which is the dominant performance indicator for this application.

5.5.2 Tower extension and wire mesh

From Figure 17 it can be deduced that for axial flow conditions, the application of the 'towertail' yields an approximate C_T reduction of 0.02. It was hypothesized that the reduced blockage in front of the tower would also result in an increased mass flow through the rotor and thus a higher C_P value. However the Figure clearly illustrates by the constant C_P value that this is not the case. Most likely the

increase in flow velocity at the cylinder sides compensates for the blockage and hence the total mass flow through the rotor is not affected.
Figure 7 shows that a reduction of 0.04 in C_T can be achieved by removal of the wire mesh in front of the rotor. The corresponding effect on C_P has not been measured although this is expected to be significant. The positioning of the mesh in front of the rotor will redirect extra mass flow outside of the rotor and hence affect the C_P value as well. Using 1D momentum theory a rough estimate can be made of the increase in mass flow through the rotor and hence in C_P. For a C_T value (with mesh) of 0.7, this would indicate an increase in mass flow rate of 2.3%. The net increase of the C_P/C_T ratio would then be 8.5%.
The figures above indicate that a significant performance increase can be achieved if both front and rear meshes can be omitted.

5.6 Comparison with predictions

Performance curves have been estimated for various pitch angles using BEM theory. It was found that application of Jamieson's theory [6] on the calculations would over predict the experimental results (C_P and C_T) consistently by more than 50%. Therefore the effect of the shroud is not taken into account. Since it can be argued that the effect of the shroud on C_P/C_T ratio would cancel out (see also section 5.4.1), the comparison is made using this variable.

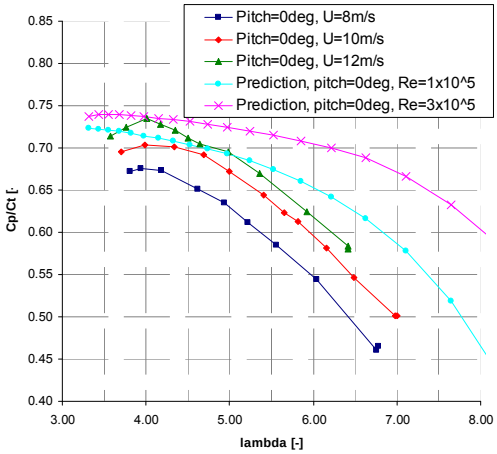

Figure 18: Comparison for pitch=0 degrees

The results for two pitch angles are shown in Figure 18 and 19. The Reynolds effect is simulated by inputting two different sets of profile coefficients. They yield an effect of the same order as measured in the tunnel.

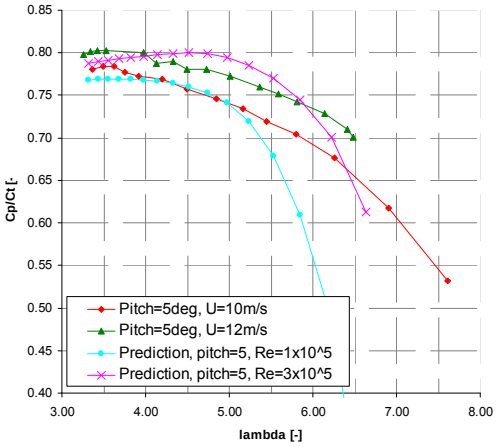

Figure 19: Comparison for pitch=5 degrees

For low tip speed ratios the agreement is satisfactory, but the shape of the curve and hence the values deviate significantly for increasing lambdas. It can be questioned whether the effect of the shroud on the displayed C_P/C_T ratio cancels out. As noted in section 3.1 the alteration of the velocity field by the shroud is not uniform over the rotor plane and local effects might cause different trends in power and thrust. A more detailed investigation is recommended (e.g. an integral simulation of the rotor-diffuser combination using vortex line theory) to come to a more final conclusion on this matter.

5.7 Model parameters of the car

The model parameters for the *Impulse* have been estimated with the performance model of Chapter 2 from measurements during the race, the rotor characteristics (C_P, C_T) for 5 degrees pitch angle at 12 m/s and the measured drag area of the other components (A_o). A_o is determined from the axial force coefficient at rotor standstill (Figure 7) and corrected for the contribution of part 3 from Figure 6 which is shielded by the car body. The mass of the car with driver was 430 kg. The results are presented in Table 2. The calculated car velocities are compared with the measured velocities during the race in Table 3.

A	rotor area	2.835
A_D	drag area of the car body	0.244
A_o	drag area other components	0.440
η	drive train efficiency	90%
M	mass of car and driver	430
f	friction coefficient	0.017

Table 2: Model parameters for the *Impulse*

wind speed	measured	calculated
8.5	3.8	3.8
9.3	4.85	4.7

Table 3: Car velocities measured during the race and calculated with the performance model.

5.8 Performance improvement

ECN was the first subscriber to the race but concrete design activities started much later. Therefore design choices in the project were dominated by rough instead of sophisticated analysis and priority for short realization paths for production and assembly. As a result many model parameters have not been optimized.
So it is interesting to estimate the vehicle speed of an improved car with the same rotor-diffuser combination.
Assume that the weight of the car could be reduced to 130 kg - just like the *Inventus* of the University of Stuttgart, one of the competitors in the race – and that the total drag area could be reduced by about 30% through reduction of the frontal area and interference, mainly of the terminal connections between mesh and diffuser. Then the total mass reduces to about 200 kg and the drag area to about 0.48 m^2.
As mentioned in section 5.5 the performance of the rotor-diffuser combination will be increased by omitting the front and rear meshes. As a result the car velocity will increase to 8.2 m/s at 9.3 m/s average wind speed.
Further increase of the car velocity has to be sought by optimizing the design of the rotor-diffuser combination.

6. Conclusions

A successful wind tunnel test campaign of a shrouded rotor has resulted in a valuable database for use in wind powered vehicle design and beyond. The results indicate that for this specific rotor the optimum performance is achieved for a pitch angle of 5 degrees at relatively low tip speed ratios of around 4. Reynolds number effects are significant for the present rotor, showing an increase of up to 10% in C_P/C_T ratio in the range of freestream velocities between 8 and 12 m/s. The removal of the front wire mesh has the potential of increasing the C_P/C_T ratio by 8.5%. The performance at small yaw misalignment (5 degrees) is hardly affected, but at 20 degrees misalignment the rotor speed is killed. Furthermore flow visualization implies that a larger opening angle of the shroud can be applied resulting in a significant increase in C_P but also C_T. A comparison with BEM predictions shows good agreement of the C_P/C_T ratio for low tip speed ratios. However large discrepancies are present between calculations and measurements for high lambdas. The absence of modeling the effects of the shroud is presented as possible cause for the discrepancy. However, a more detailed investigation is recommended to come to a more final conclusion on this matter.

Analysis with the model for the car performance shows that 88% of the wind speed can be achieved with the same rotor-diffuser combination at realistic reductions of the total weight of the car and its frontal area and by improving the C_P/C_T ratio only by omitting the wire mesh.

Acknowledgements

The authors would like to express their gratitude to Delft University of Technology and more specifically to Nando Timmer for opening up the possibility to use the OJF. Furthermore the contribution to the realization of the test model by Rudolf Hoep, Ton Ruiter, Erwin Werkhoven and Geert Hanraads of ECN was greatly appreciated.

References

[1] Gaunaa, M. and Øye, S. and Mikkelsen, R. “Theory and Design of Flow Driven Vehicles Using Rotors for Energy Conversion”, Proceedings EWEC 2009, March 16-19, Marseille, France.

[2] Hoerner, S.F., Fluid-dynamic drag, Published by the author, 1965

[3] Ewald, B.F.R., AGARDograph 336, Wind tunnel wall correction, Canada communication group Inc., October 1998

[4] Barlow, J.B. and Rae, W.H. jr. and Pope, A., Low-speed wind tunnel testing, third edition, John Wiley & Sons Inc., 1999

[5] Snel, H. and Houwink, R. and Bosschers, J. and Piers, W.J. and Van Bussel, G.J.W., “Sectional predictions of 3-d effects for stalled flow on rotating blades and comparison with measurements”, Conference proceedings European Wind Energy Conference, Lübeck-Travemünde, Germany, March 1993

[6] Jamieson, P.M., “Beating Betz: energy extraction limits in a constrained flow field”, Journal of Solar Energy Engineering, Vol 131, Issue 3, 2009